Original article

Unique nasal septal island in dromedary camels may play a role in pain perception: microscopic studies

Ahmed I. Abo-Ahmed [a], Eman A. Eshrah [a], Fatgzim Latifi [b],*

[a] Department of Anatomy and Embryology, Faculty of Veterinary Medicine, Benha University, Toukh 13736, Egypt
[b] Department of Veterinary Medicine, Faculty of Agriculture and Veterinary, University of Prishtina "Hasan Prishtina", Prishtina, Kosovo

ABSTRACT

The septal organs are islands or patches of sensory epithelium, located in the ventral parts of the nasal septum and innervated by the olfactory nerve. The septal island in dromedaries (*Camelus dromedarius*) was unusually located in the rostro-dorsal part of the nasal septum, where the ethmoidal branch of the trigeminal nerve provides innervation to the island mucosa. Therefore, the objectives of this study were to reveal the microscopic and ultrastructure of this island and to explain the probable functions. Twelve septal islands from 12 healthy male camels were used. Unlike the olfactory epithelium, which has a pseudostratified structure, the island neuroepithelium had a true neural lamination. Furthermore, in electron micrographs, the receptor, bipolar, and basal cells were connected with an orderly, organized network of cell–cell communication, which had some spine synapses. This network substituted the absence of supporting cells, maintained the shape of the tissue, and held the cells together. Moreover, the receptor cells were not similar to any of the different types of olfactory sensory neurons. Instead, they possessed the apical domain that might be specialized for the detection of chemical stimuli. Interestingly, a resident population of immune cells, namely mast cells and macrophages, was observed. The probable functions were discussed based on the cellular context and architecture. The nasal septal island in dromedaries may have a role in pain perception. The receptor cells most probably work as nociceptive cells that interact with the resident immune cells to coordinate pain signaling with immune response.

1. Introduction

One of the essential components in each sensory epithelium is the receptor cells that receive and transform signals from the external environment (odors, light, sound, and tastants) into electrical impulses that can be interpreted in the nervous system (Alberts et al., 2002). The nasal cavity of all vertebrates houses multiple receptor cells, either innervated by the olfactory or the trigeminal cranial nerve (Hansen, 2007). They intermingle in one epithelium in non-mammalian vertebrates (Hansen, 2007). However, in the mammalian nose, the trigeminally innervated sensory cells are "solitary chemosensory cells" (Krasteva & Kummer, 2012). They are scattered in the upper respiratory tract, including the nasal respiratory mucosa, vomeronasal duct, and auditory tube, and they all monitor the chemical composition of the mucosal lining fluid (Krasteva & Kummer, 2012). Conversely, the olfactory receptor cells, innervated by the olfactory nerve, are either ciliated or microvillar sensory cells (Farbman, 1992). They are segregated into three compartments, which are the olfactory mucosa, the vomeronasal organ (VNO), and the septal organ of Masera (SOM).

The SOM is a specific chemosensory organ observed only in some mammalian species (Ma et al., 2003). Typically, it is a small, isolated patch or island of sensory cells, a few hundred micrometers in diameter, located bilaterally in the ventral part of the nasal septum in some marsupial species (Kratzing, 1984), hamsters (Taniguchi et al., 1993), rats (Weiler and Farbman, 2003), and the domestic cat (Kociánová et al., 2006). In contrast to the SOM, the Grüneberg ganglion (GG) has been described as a septal organ only in the murine nose. Moreover, it lacks typical sensory epithelia, and instead, the GG cells that form special aggregations in the lamina propria have no direct access to the nasal lumen (Storan and Key, 2006).

When asked about "nasal septal organs," most researchers initially refer to the sense of smell and link them to the olfactory pathways. This contributes to the fact that the terminal axons of the nasal septal organs project to the olfactory bulb (Marshall and Maruniak, 1986; Giannetti et al., 1992; Fuss et al., 2005), and the ability of sensory cells to express a handful of odorant-binding proteins (Fleischer et al., 2006; Brechbuhl et al., 2008; Grosmaitre et al., 2009). However, they are also receptive to other sensory modalities mediated by mechanical (Grosmaitre et al., 2007) and thermal stimuli (Mamasuew et al., 2008; Mamasuew et al., 2010).

The authors have noticed a septal island within the soft tissue of dorso-rostral parts of the nasal septum during the examination of the nasal cavity in camels. It can be recognized macroscopically because of its dark pigmentation. Accordingly, the authors took preliminary tissue samples, in the belief that it might have special glands beneath the surface epithelium, giving the tissue its distinctive dark color. The preliminary examination comes as expected and, the septal island was formed of neuroepithelium with distinct subepithelial and submucosal glands.

To the best of our knowledge, the available literature has not reported any information regarding the presence of sensory epithelium in such location in any mammalian species. Therefore, the aim of the present study was to describe in detail the topographic anatomy and nerve supply of this neuroepithelium, the fine and ultra-structure using light and electron microscopy, and speculate the possible functions.

2. Materials and methods

2.1. Samples

This study was performed in accordance with the ethical guidelines approved by the Institutional Animal Care and Use Committee of Faculty of Veterinary Medicine, Benha University, Egypt. The study was conducted on 12 paired organs from 12, three- to six-years-old apparently healthy mature male dromedaries (*Camelus dromedarius*). The specimens were obtained immediately after slaughter from the Toukh and Qalioube abattoir, Egypt. Congenital or acquired abnormalities of the nose or nasal septum were considered to be exclusion criteria. Two heads were used for gross anatomy, while the other ten heads were used for light and electron microscopy.

2.2. Light microscopy (LM)

Histological samples were obtained immediately after slaughter, the dark pigmented septal island was dissected and cut into blocks to obtain transverse, sagittal, and oblique sections. The tissue blocks were fixed in 10% neutral buffered formalin, dehydrated in an ascending series of alcohol (70 to 100%), cleared in xylene, and embedded in paraffin. In addition to the formalin-fixed samples, some tissue blocks were fixed in 4% buffered glutaraldehyde at pH 7.2. These blocks were subsequently processed as described above and embedded in paraffin. Three μm thick sections were mounted on glass microscope slides, deparaffinized, and stained with hematoxylin and eosin (H&E) and Mallory's trichrome (Bancroft and Stevens, 1997).

2.3. Scanning electron microscopy (SEM)

The mucosal surface of the septal organ was washed carefully in normal saline, then, small pieces of fresh specimens were cut and fixed in glutaraldehyde, pH 7.4, at 4 °C for three hours. The fixed specimens were washed three times (10 min each) in phosphate-buffered saline (PBS), post-fixed in 1% osmium tetraoxide for 30 min at room temperature, and then dehydrated with an ascending series of ethyl alcohol (30, 50, 70, 90%, and absolute alcohol), then infiltrated with acetone. The tissues were immersed in each solution for 30 min. Samples were dried in a Samdri-PVT-3B® (Tousimis, Rockville, USA), critical point drying machine using liquid CO_2, mounted on aluminum stubs, and coated with gold to a thickness of 0.04 μm in a sputter-coating unit (JFC-1100 E). Finally, observations of the septal organ morphology in coded specimens were performed using a Jeol-JSM- 5300 LV scanning electron microscope (Tokyo, Japan) at 20 KV in the electron microscopy unit at Alexandria University, Egypt.

2.4. Transmission electron microscopy (TEM)

Small pieces of fresh specimens were fixed in 4% buffered glutaraldehyde, pH 7.2, at 4 °C for three hours. Post-fixation was carried out in 1% osmium tetraoxide followed by dehydration in graded series of acetone at 4 °C. The tissues were embedded in resin and cut into sections approximately 0.009 μm in thickness. Semithin sections were stained with 1% toluidine blue and 1% sodium borate (borax) in 100 ml distilled water. Ultrathin sections were immersed in uranyl acetate for 5 min, then lead citrate for 2 min to enhance the contrast and examined using a JEOL-JSM-1400 PLUS electron microscope (Tokyo, Japan) in the electron microscopy unit, Alexandria University, Egypt.

3. Results

3.1. Gross structure

The septal island in dromedaries appeared as a dark pigmented area, in which the mucosa was brownish of different degrees of intensity, 8–14 mm in length (mediolateral extension) and located bilaterally in the rostro-dorsal part of the nasal septum (Fig. 1a, b). It could be divided into two parts, septal and paraseptal or dorsal. The latter was the dorsolateral continuation of the septal portion of the adjacent nasal mucosa (Fig. 1a). Topographically, the island was located 5–6 cm caudomedial to the lateral nasal angle. Internally, it started to appear 2.5–3 cm caudal to the rostral end of the straight fold, which related dorsolaterally to the island (Fig. 1a). The mucosa was innervated by branches of the ethmoidal
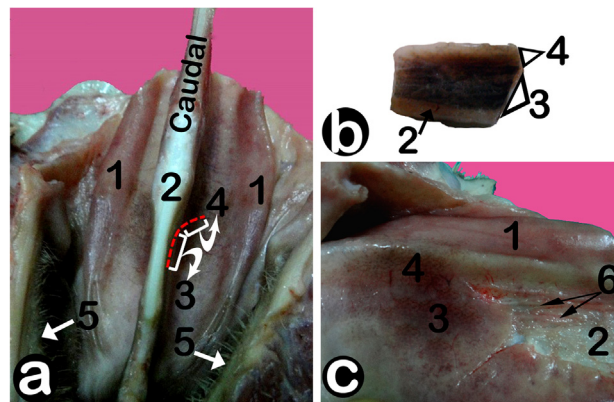

Fig. 1. Gross anatomy of the nasal septal island in dromedaries: **(a)** Ventral view of the nasal vestibule showing the location and relationships of the nasal septal island (red dashed line), **(b)** The nasal septal island (excised), **(c)** Nerve supply of the septal island. The straight fold of the dorsal nasal concha (1), the nasal septum (2), the septal part of the island (3), the paraseptal (dorsal) part of the island (4), the inner side of the nostril (5), and branches of the ethmoidal nerve (6).

nerve of the ophthalmic division of the trigeminal nerve (Figs. 1c and 2).

3.2. Fine structure

The neuroepithelium of the septal island was a multilayered structure consisting of a stratified columnar epithelium with well-developed glandular and vascular tissue. It was clearly
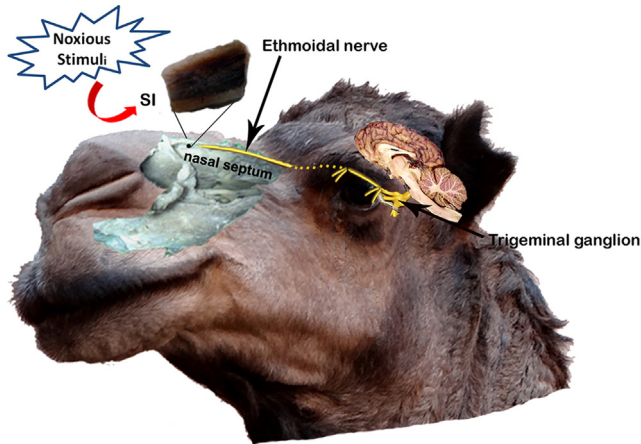

Fig. 2. Schematic representation of the camel head showing the location and nerve supply of the septal island (SI).

defined from the surrounding keratinized stratified epithelium, which lined the rostral (vestibular) part of the nasal septum (Fig. 3a, b).

Histologically, the neuroepithelium consisted of the distinct upper, middle, and basal cell layers, which decreased in height toward the dorsal paraseptal region (Fig. 3c, d). Although these different layers were visible with H&E, the trichrome stain displayed contrasting colors that allowed better demonstration of the upper layer cells. In contrast to the bipolar cells of the middle layer that were either unstained or appeared pale, the apical (receptor) cells were intensely red with trichrome staining (Fig. 3a).

The upper layer consisted of a monolayer of smaller, intensely stained cells with different morphological types. Some cells were round to cylindrical with a round central nucleus, and others were pear-shaped cells with a large basal nucleus. These types were inconstant, and their incidence varied regionally in the neuroepithelium (Fig. 3c, d).

The middle layer of cells consisted mostly of bipolar cells with two recognizable groups, in which cells with either an euchromatic (type 1a) or heterochromatic nucleus (type 1b) were seen. The euchromatic cells formed the upper two-thirds of the neuroepithelium in the septal part (Fig. 3c), while the heterochromatic cells were dominant in the paraseptal part (Fig. 3d). In type 1b cells, the heterochromatin was organized in a characteristic cartwheel or clock-face arrangement. Some of the nuclei stained with eosin. The cytoplasm revealed a pale Golgi zone next to the nucleus (Fig. 3c, d). In addition to the bipolar cells, spindle-shaped cells with arborized, branched processes (type 2) were seen sporadically along the uppermost part of the middle layer. These cells
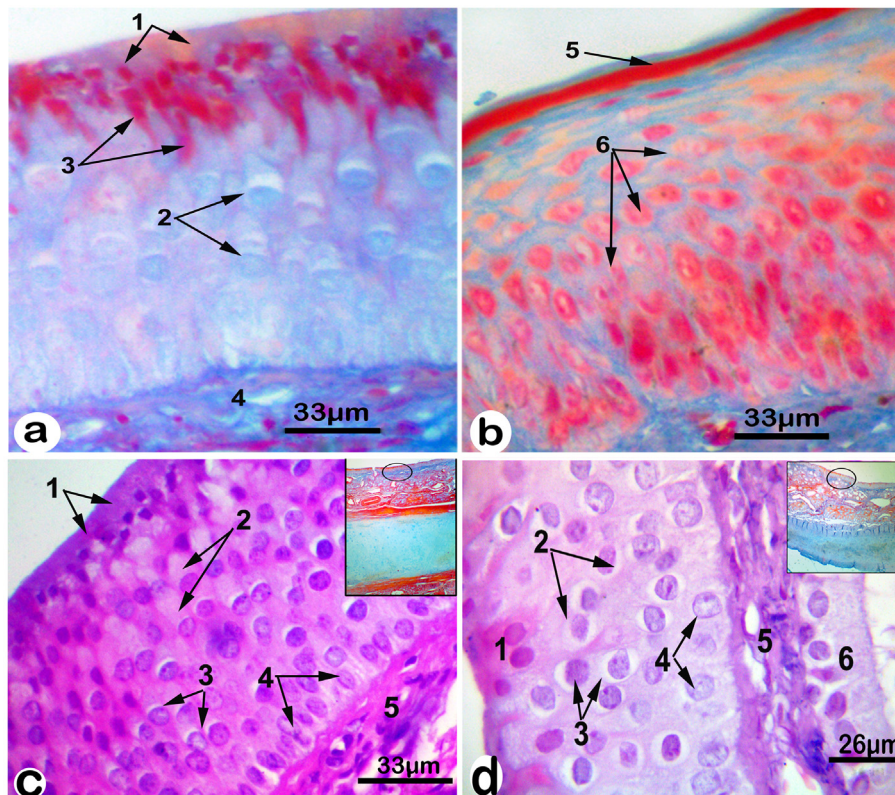
Fig. 3. Light micrographs showing (**a & b**) the neuroepithelium of the nasal septal island (septal portion) vs. the epithelium covering the nasal septum (surrounding epithelium), respectively, with Mallory's trichrome stain, X 400; apical cells (1), bipolar cells (2), spindle-shaped interconnecting cells (3), lamina propria (4), the keratin layer of the surrounding epithelium (5), keratinocytes (6). Notice that the bipolar cells are stained pale blue, while the keratinocytes of the surrounding epithelium are orange-red. (**c & d**) The layered structure of the neuroepithelium of the septal portion of the nasal septal island vs. the paraseptal portion, respectively, with H&E, X400 (inset showing all layers stained with trichrome); apical cells (1), bipolar cells (2), bipolar cells with heterochromatic nuclei (3), basal cells (4), lamina propria (5), and subepithelial glands (6). scale bar = 33 μm (**a, b, c**), 26 μm (**d**).

interconnected with the cells lying above (receptors) and the underlying (bipolar) cells (Fig. 3a, c).

The basal layer was a monolayer composed of round to oblong shaped cells with large, spherical nuclei (Fig. 3c, d). While it was difficult to recognize any melanocytes in the histological sections, the neuroepithelium and the acinar cells of subepithelial glands were heavily infiltrated with melanin pigment.

Notably, a population of immune cells was distributed throughout the lamina propria. Although they were resident cells, seen in all sections, some cells appeared to be wandering cells in a state of motion rather than "steady-state" infiltrated cells (Fig. 4). Most of these cells were fixed in the process of spreading their pseudopodia-like extensions or squeezing themselves across the capillary wall (Fig. 4). Numerous mast cells were located in the
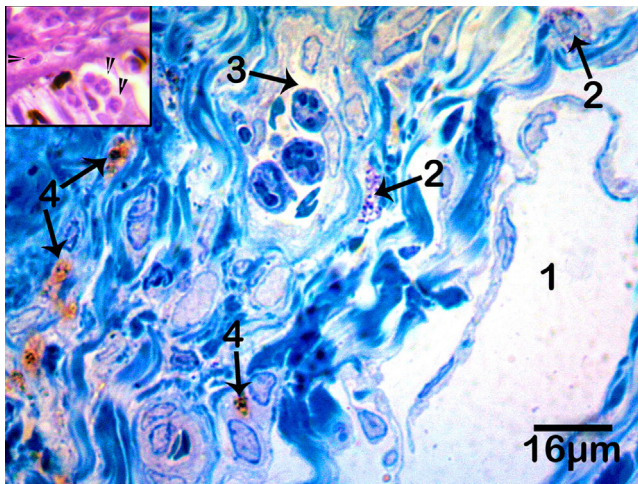
sub-epithelium and around capillaries. The characteristic metachromatic granules of mast cells were observed in toluidine blue (TL) stained sections. Also, some mononuclear phagocytes showed brownish yellow granules and endosomes that obscured the other cell organelles (Fig. 4).

Three sets of glands were associated with the sensory epithelium, including submucosal (septal glands), subepithelial, and intraepithelial glands. The submucosal glands (Fig. 5a) were compound tubuloacinar glands, which formed a continuous glandular layer that increased in thickness toward the septal region. Their secretory portions were oriented parallel to the surface, whereas the excretory ducts adopted a perpendicular course and opened onto the surface epithelium. The subepithelial glands (Fig. 5b) were abundant in the dorsal (paraseptal) part and were present to a significant extent on the septal part, predominantly in the lamina propria. Multicellular intra-epithelial glands were mainly observed in the transitional region, where the septal part adjoins the dorsal region and the transitional epithelium. They were located as clusters or nests within the surface epithelium (Fig. 5c).

Numerous wide, thin-walled vessels and venous sinuses were present in the submucosa (Fig. 5d), and they were relatively abundant in the septal part. Together with the submucosal connective tissue, they formed a sponge-like cavernous layer, which increased in thickness toward the septal region.

3.3. Scanning electron microscopy

The epithelium covering the surface was highly undulating in appearance, and formed a continuous sheet of simple elongated folds arranged in rows with intersected shallow grooves and crypts (Fig. 6a, b). Numerous glandular openings of various sizes were present, interposed between the mucosal folds, as wide cavern-like openings, medium-sized openings, and smaller openings. The small-sized openings were observed at or near the base of the mucosal folds (Fig. 6b). The cavernous openings were unusually wide, bulged slightly from the underlying epithelium, and smaller
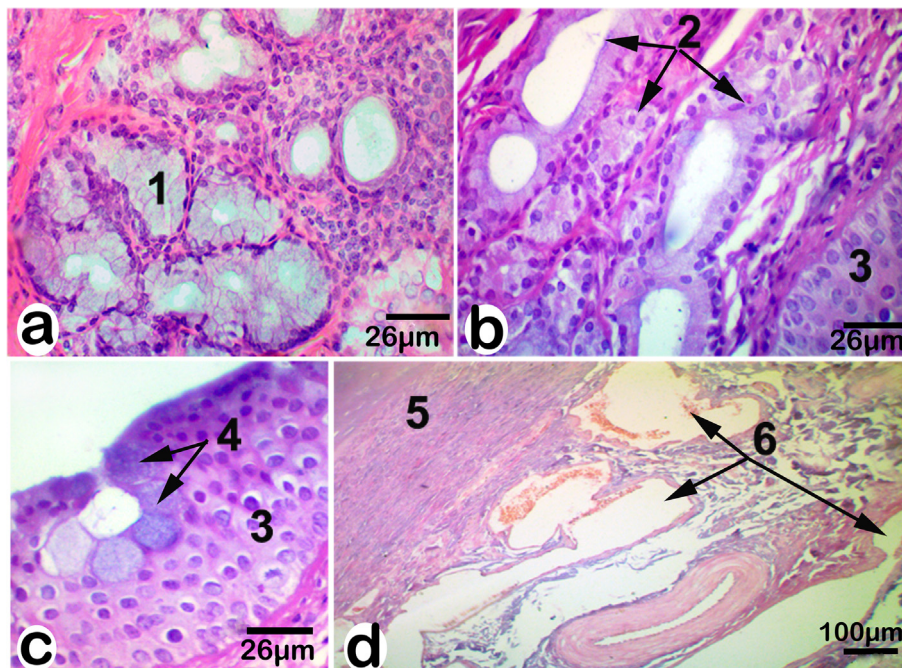

Fig. 4. Light micrograph of the lamina propria of the nasal septal island stained with Toluidine blue, showing lymphatic capillaries (1), mast cells (2), wide blood capillaries (3), mononuclear phagocytic cells with yellow–brown granules (4), and inset showing some multinucleated phagocytic cells.

Fig. 5. Light micrographs of the glands of the nasal septal island in dromedaries **(a-c)** H&E, X 400, showing some seromucous acini of the submucosal glands (1), the subepithelial glands (2), the neuroepithelium (3) the intraepithelial glands within the sensory epithelium (4). **(d)** The vascular tissue (pump), H&E, X100, the perichondrium of the nasal septal cartilage (5), wide, thin-walled blood vessels (6).
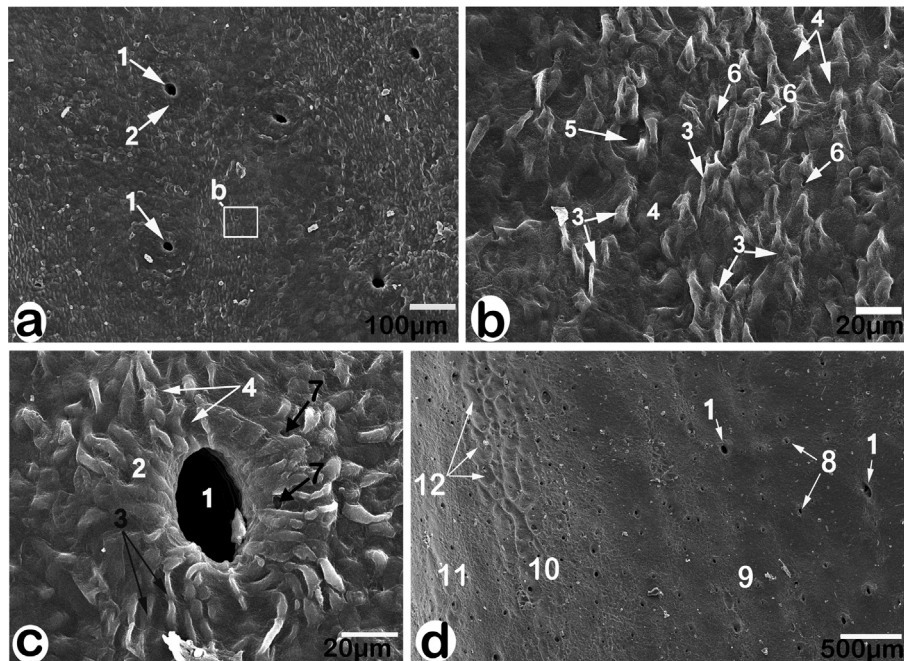
Fig. 6. Scanning electron micrographs showing the surface appearance of septal islands in dromedaries X 120 (**a**), the arrangement of the mucosal folds, X 650 (**b**), the mucosal rosette around cavernous glandular openings, X 800 (**c**), the distribution of the glandular openings, X 30 (**d**): the cavern-like openings (1), mucosal rosette (2), simple elongated mucosal folds (3), intermucosal grooves (4), shallow crypts (5), small-sized glandular openings (6), smaller foramina in the glandular opening rim (7), medium-sized glandular openings (8), the epithelium covering main area of the septal organ (9), a transitional zone (10), the nasal mucosa surrounding the septal organ (11), well-communicated troughs around the medium-sized glandular openings (12).

openings penetrated the rim (Fig. 6a, c). Each cavernous opening was surrounded by a mucosal rosette, in which the mucosal folds alternated with the grooves (Fig. 6a, c). Continuing distally towards the transitional epithelium, shallow troughs appeared around the medium-sized openings, which were well-developed and communicated at the transitional zone (Fig. 6d).

3.4. Transmission electron microscopy (TEM)

Nissl bodies were seen within the bipolar cells as coarse, deeply basophilic (orthochromatic) granules in semithin preparations. The cell bodies were arranged in an organized fashion, forming a complex cellular network, in which cell junctions had a peculiar punctuate appearance (Fig. 7a, b).

TEM revealed unique cell to cell communications, where desmosomes existed in an alternating manner with spines, giving the cell boundaries a characteristic punctate or stippled appearance. These desmosomes attached the cells at distances that allowed intercellular communication fields to occur, each of which was approximately 0.3–0.5 μm in width and 1.5–2 μm in length (Fig. 7b, c). Within each communication field, the plasma membranes of the adjacent cells presented many small, parallel spiny projections, with their free ends often convexly curved toward each other (Fig. 7b, c). An active zone was present where numerous vesicles were clustered, in addition to a variable number of mitochondria, few ribosomes, and rough endoplasmic reticulum (RER) tubules (Fig. 7b). The vesicles were spherical, 83–167 nm in diameter, and had a homogenous, moderate electron density appearance (Fig. 7b). Some vesicles were fused with the cell membrane, and their lumen opened into the intracellular space (Fig. 7b).

Notably, some of the small projections were typical neural spines; each had a large head connected to the plasmalemma via a membranous neck (Fig. 7d). Moreover, at higher EM magnifications, some synaptic spines were visible. The spine heads showed typical protein densities with a synaptic cleft of 11–12 nm and an intracellular space filled by an electron-lucent substance (matrix) (Fig. 7d).

The apical domains mostly contained microvilli with an electron-dense coat (Fig. 8a, b). Whereas, the uppermost parts of the adjacent apical cells had tight junctions (Fig. 8b). Numerous early endosomes were also seen in the most peripheral region of these cells (Fig. 8a, b). The pear-shaped apical cells possessed very short axon-like basal process, which communicated with both the bipolar cells and the type2 cells.

The middle layer of cells was mostly formed of bipolar cells, and each cell had proximal and distal processes that extended from a central soma (Fig. 8c). These processes were 0.9–1.7 and 1.5–1.7 μm in thickness, respectively, whereas, the cells body was 2.2–2.9 μm in diameter and typically was not much larger than the cell nucleus it contained.

The bipolar cells had organelles that are normally present in any neuron. The Nissl bodies consisted of RER in ordered parallel arrays and ribosomes arranged in rows and clusters (Fig. 8d, e). Spheroid shaped mitochondria with irregular cristae, 222–306 nm in diameter were present, and they were especially numerous in the distal endings of the cells (Fig. 8e). Moreover, the melanin pigments were not dispersed in the cytoplasm. Instead, they were localized in the prenuclear area to form a melanin organelle (MO) (Fig. 8c, d). Within each MO, the melanin pigments were organized as spherical granules with high electron density, which often were associated with electron-lucent bodies (Fig. 8d, e). These melanin granules were smaller, 278 to 388 nm in diameter, and more spherical compared with those found within the pigmented processes of melanocytes.

The columnar and horizontal organization of the neuroepithelium was very complex. Therefore, it was challenging to define a fundamental unit of organization. However, some essential cellular relations were revealed, in which the pear-shaped receptor cells communicated with the underlying bipolar cells through a very short axon-like basal process (Fig. 9a, b). Additional interconnec-
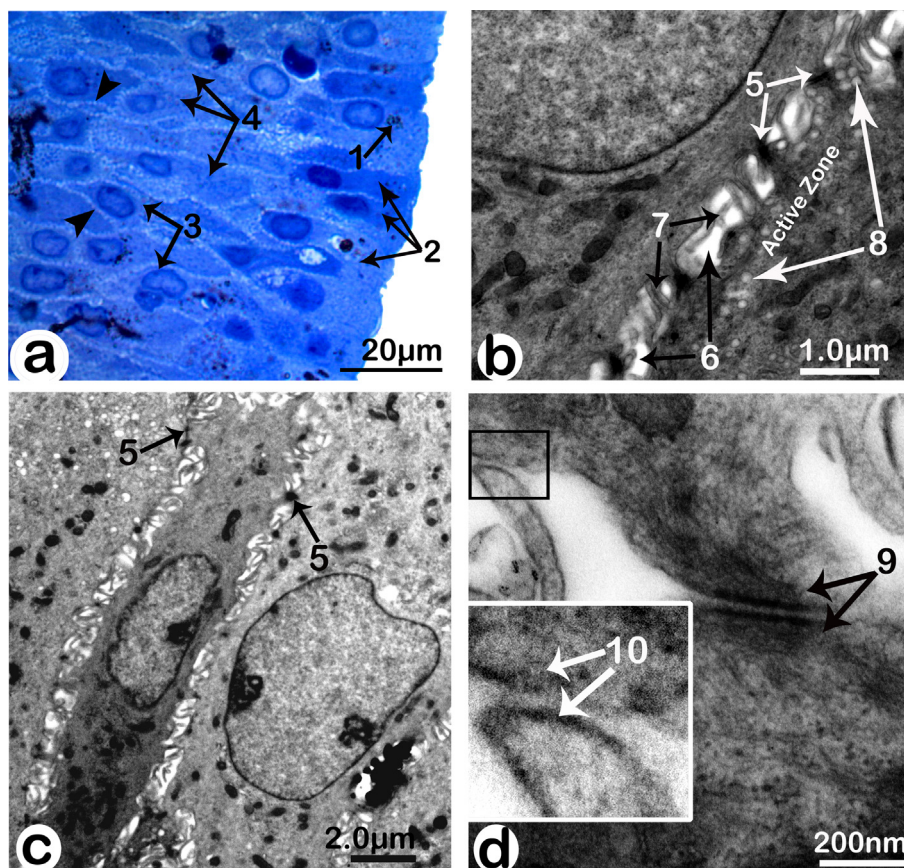
Fig. 7. (a) Semithin micrograph of the neuroepithelium showing the cell to cell communication network, which has a punctate appearance (black arrowheads), melanin organelle in the supranuclear region (1), the apical cells (2), bipolar nerve cells (3), distribution of Nissl granules in the bipolar cells (4). **(b, c & d)** Electron micrographs of the neuroepithelium showing the desmosomes (5), communication fields (6), finger-like processes or spines within each communication field (7), the active zone, where synaptic vesicles are clustered (8), terminal web of desmosomes (9). Inset of (d) showing the spine heads and density of spine synapses (10).

tions were provided by the type 2 cells through their plexiform processes (Fig. 9a).

The basal cell layer was composed of round cells with large irregular nuclei and mitochondria-rich cytoplasm (Fig. 9c). The basement membrane was notably thick with a homogenous glassy appearance. Few melanocytes with poorly developed dendrites were observed above the basement membrane and between the basal cells (Fig. 9c). At the level of the lamina propria and just beneath the basement membrane, some unmyelinated, somatosensory afferent nerve fibers were observed and they were surrounded by a belt-like cluster of Merkel- Ranvier cells (Fig. 9d). Besides, the dilated nerve terminals were seen between the basal cells (Fig. 9d).

4. Discussion

The present study revealed a novel septal island (SI) in dromedaries. It was located rostro-dorsally on the nasal septum 5–6 cm caudomedial to the lateral nasal angle and 2.5–3 cm caudal to the rostral end of the straight fold and innervated by the ethmoidal nerve, in the region where intranasal trigeminal chemosensitivity occurs. Some functional magnetic resonance studies have shown that intranasal trigeminal stimulation activates the entire area responsible for pain sensation or nociception (Boyle et al., 2007; Iannilli et al., 2008; Seifert and Maihofner, 2009; Albrecht et al., 2010; Lundström et al., 2011). This activation might be related to the hypothesis reported by Lötsch et al. (2020) where the intranasal trigeminal stimuli activate the branches of trigeminal ganglion

cells projected into the nociceptive neurons of the piriform cortex as well as secondary somatosensory cortex which are involved in encoding the subjectively perceived intensity of chemosensory trigeminal stimuli and play a major role in trigeminal pain perception. Moreover, it has been confirmed that the ethmoidal nerve possesses well-developed responsiveness to noxious stimuli such as chemical irritants and chemical mediators from C-fiber endings (Sekizawa and Tsubone, 1994).

With respect to the cellular context and nerve supply, the authors hypothesized that the SI in dromedaries is specialized for functions related to trigeminal senses, particularly pain perception. The morphology of receptor cells and the anatomically associated immune cells, namely mast cells and macrophages, support this hypothesis. Mast cells and macrophages normally colocalize with nociceptors, where they contribute to the cellular response to noxious stimuli (Aich et al., 2015; Chatterjea and Martinov, 2015; Pinho-Ribeiro et al., 2017). To highlight this information, we discuss the structure of the SI tissue in relation to its possible functions.

At the LM level, trichrome was not only useful as a differential (special) stain but also to demonstrate the structure of the neuroepithelial layers. The cells of the upper layer stained intensely with acid fuchsine, i.e., the red dye in Mallory's trichrome. Acid fuchsin stains potential protein deposits bright red, including sensory proteins, transporter proteins, and synthetic enzymes (Bancroft and Stevens, 1997). On the other hand, the bipolar cells appeared pale or unstained, very similar to the chemosensory cells of the taste buds located in the camel epiglottis (Eshrah and Kassab, 2019).
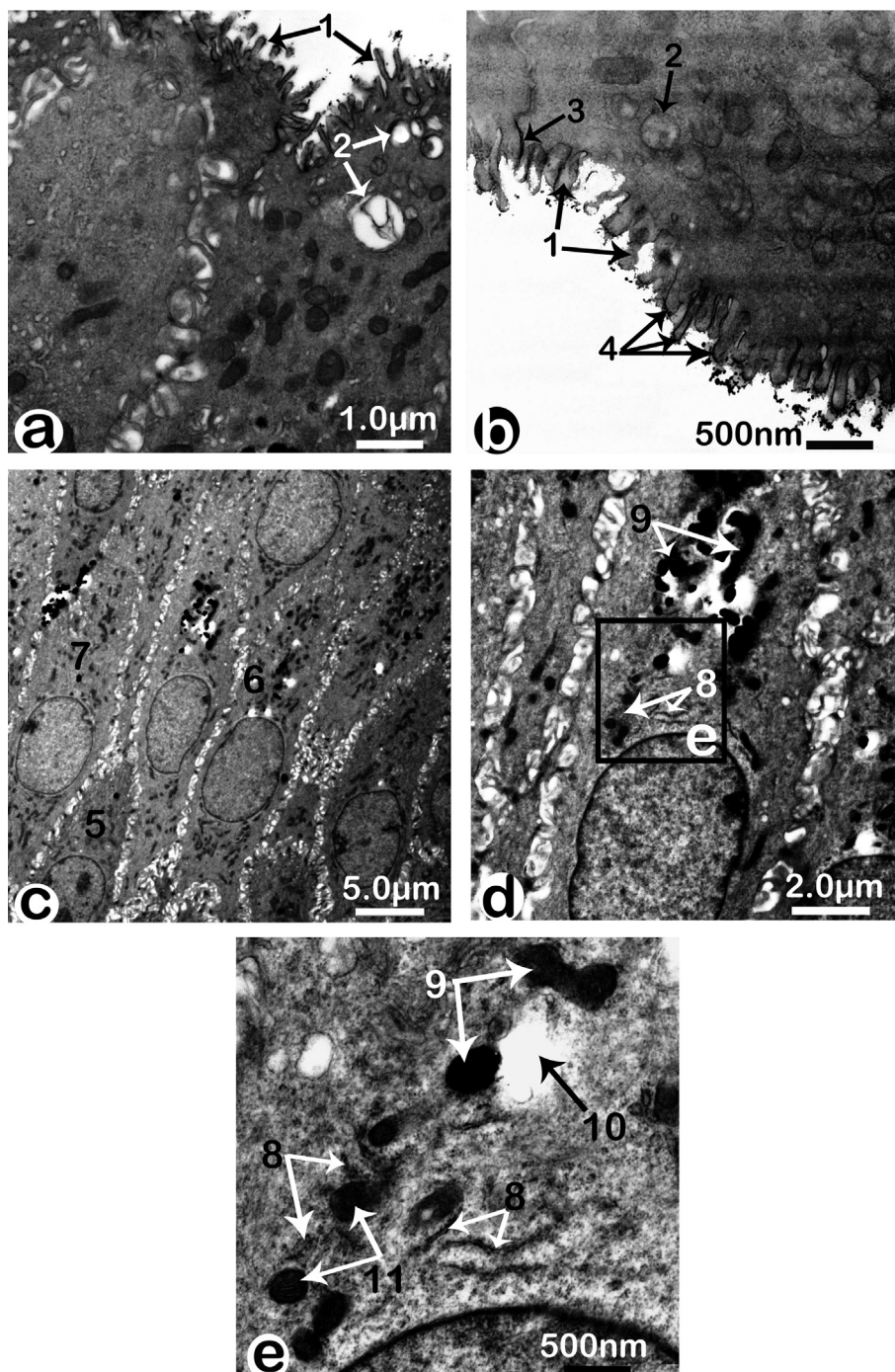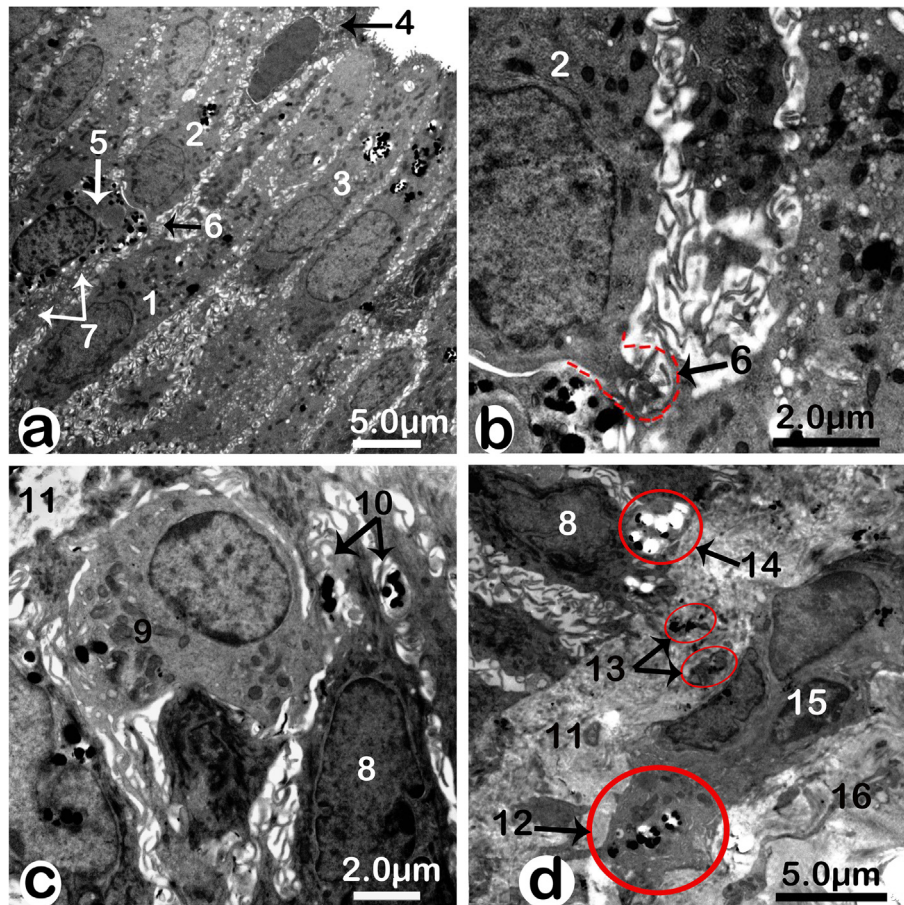
Fig. 8. Electron micrographs of the neuroepithelium showing **(a)** the upper cell layer, and **(b)** the apical modification (microvilli). Note the microvilli (1), early endosomes (2), tight junctions (3), an electron-dense coat (4), (**c**) Showing heterochromatic bipolar cells (5), the dendrites of the euchromatic bipolar cells (6,7), **(d & e)** Bipolar cells showing distribution of Nissl granules (8), melanin organelle (9), the electron-lucent bodies that are associated with melanin granules (10), mitochondria (11).

At the EM level, it was clear that the morphology of the SI neu-roepithelium did not fit the olfactory scheme. The olfactory epithelium has a pseudostratified structure, in which basal, supporting, and receptor cells are arranged side by side along the vertical axis of the epithelium (Nomura et al., 2004; Chen et al., 2014). In contrast, the SI epithelium lacked the supporting cells. The SI epithelium showed a true stratification (lamination), in which receptor, bipolar, and basal cells were arranged, along the horizontal axis of the epithelium.

As their name implies, supporting cells hold cells together because they occupy the full length of the epithelium and have branched foot processes spreading on the basal lamina (Nomura et al., 2004). The presence of a network of communication junctions in the SI tissue substitutes functions of supporting cells. Although they were fundamentally different, except for the presence of desmosomes, these junctions had a spiny appearance that could be mistaken for the prickle cell layer. The prickle cell spines (PCS) were visible with traditional staining at higher LM magnifications (Fawcett and Jensh, 1997), but the SI spines (SIS) were not. Also, the PCS are cell bridges that cross each other in an interdigitating manner, and the cells adhere to tight fusion (Fawcett and Jensh, 1997; Eshrah, 2017). The SIS were sites where two cells were

Fig. 9. Electron micrographs of the neuroepithelium showing **(a)** the columnar organization of the tissue. Note the bipolar cells (1), the pear-shaped receptor cells (2), cylindrical receptor cells (3), a triangular-shaped apical cell (4), type 2 cells (5), very short axon-like basal process of the pear-shaped cells (6), and the interconnecting plexus of the type 2 cells (7). **(b)** Magnification of the pear-shaped receptor cells showing their very short axon-like basal process (6). **(c)** The basal cell layer showing basal cells (8), a melanocyte (9), pigmented processes of the melanocyte (10), the basement membrane (11). **(d)** Showing the nerve fiber (unmyelinated) (12) and parts of the nerve fiber (13) at the basement membrane (11), nerve terminal (14), a belt-like cluster of Merkel-Ranvier cells surrounding the nerve fiber (15), and lamina propria (16). Notice that the Merkel-Ranvier cells substitutes the absence of myelin sheath, and as many other somatosensory afferents, the nerve fiber has a dilated terminal just beneath the basal cells.

adhered without fusion, and some of them carried typical synapses that were revealed only with TEM.

The SIS showed the morphological hallmarks of chemical synapses. This included increased electron density in opposing areas of the cell membranes, clusters of synaptic vesicles close to a dense region of the membrane, and a slight increase in the width of the extracellular space (11–12 nm) (Dustin and Colman, 2002). In this sense, the spine synapses in the SI tissue might serve to increase the number of possible contacts between neurons, and thereby, provide fields of anatomical communication, allowing memory storage and synaptic transmission. This presumably allows synchronous receiving and processing of sensory information (Wu, 2010; Kubota et al., 2016), which is an indicator of a functional context not related to the traditional categories of smell or taste.

Another curious observation was the abundance of melanin pigments, which were found intracellularly in melanin organelles, and the processes of melanocytes. This accounts for the brownish appearance of this region.

The SI receptor cells were morphologically similar to the solitary microvillar chemosensory cells of the upper airways, which are also innervated by the trigeminal nerves (Hansen, 2007). These chemosensory cells serve as sentinels detecting bacterial colonization or the presence of other harmful components in the mucosal lining fluid (Krasteva & Kummer, 2012). On the other hand, the

SI receptor cells were not structurally similar to the different olfactory sensory neurons, including ciliated, microvillus, and crypt neurons (Hansen and Zeiske, 1998).

Typical for neuron cells, the SI bipolar cells possessed Nissl substance, which was abundant in the dendrites and absent in the axon hillock, multivesicular bodies (Siegrist et al., 1968, Banks, 1993), and mitochondria, which were typically spheroid and had irregular cristae (Fawcett and Jensh, 1997). The arrangement of the RER, mitochondria, and nuclei suggested that these cells were active in protein-glycoprotein synthesis (Fischer et al., 2008). Like many other neural cells, these protein substances are a part of the signaling cascade. By virtue of their communication with SI receptor cells, bipolar cells possibly act as a second-order neuron. After being activated by the receptor cells, they might secrete their signaling factors, which would help maintain tissue sensitization after the initiating stimulus was terminated. This feasible mechanism of sensitization is considered a feature of nociception perception (Llewellyn McKone, 1997).

The SI glands occurred in three sets, subepithelial, submucosal, and intraepithelial glands. Scanning electron microscopy revealed unusually wide glandular openings similar to those associated with the taste buds of the epiglottis in camels (Eshrah and Kassab, 2019). This suggests that the submucosal glands have their secretions aerosolized, rather than coating the surface; i.e., the glandular secretions might convert into a fine spray or colloidal

suspension in the air (Widdicombe and Wine, 2015). Multicellular intraepithelial glands are rare in respiratory airways. Instead, they are usually present in the genital system, including the urethra (Banks, 1993) and the epididymis of the camel (Abdel-Maksoud et al., 2019). Recent studies defined the intraepithelial glands in VNO of the brown bear (Tomiyasu et al., 2017; Tomiyasu et al., 2018) and humans and chimpanzees, (Smith et al., 2002) in humans and chimpanzees. They were also found in the nasopalatine duct of the brown greater Galago, *Otolemur crassicaudatus* (Smith et al., 2002). However, the function of these intraepithelial glands is still unknown. Together, cellular context and nerve supply of the SI tissue indicate sensation modalities, which do not fit into the traditional sense categories of chemoreception, i.e., taste and smell. However, it can be involved in pain perception associated with trigeminal intranasal chemosensitivity.

Finally, the SI tissue has the machinery required to detect and process sensory information. The feasible mechanism of action could be explained as follows: The receptor cells might act as nociceptive cells, where the microvilli-glycocalyx coat received the stimulus and initiate the signaling cascade. These signals probably sensitize the underlying bipolar cells via the cell to cell communication network, causing a synchronous release of chemical factors to maintain tissue sensitization, and modulate the function of resident immune cells. Consequently, the pain signals would be coordinated with the immune response. The continuous stream of the secretion from the glands would remove the remaining stimulating substances and keep the receptors ready for new stimuli.

5. Conclusion

The septal island in dromedaries is a novel anatomical structure. The cellular architecture, anatomically associated immune cells, and the nerve supply indicate that this epithelium might be specialized for nociception. This study can be used as a basis for further investigations, particularly those concerning immunoneurology as well as comparative and developmental anatomy of this region.

Declaration of Competing Interest

The authors declare that they have no known competing financial interests or personal relationships that could have appeared to influence the work reported in this paper.

Acknowledgement

Ethical approval

This article does not contain any studies with animals performed by any of the authors.

Data availability

The data that support the findings of this study are available from the first author upon reasonable request.

References

Abdel-Maksoud, F.M., Hussein, M.T., Abdelraheim, A., 2019. Seasonal variation of the intraepithelial gland in camel epididymis with special reference to autophagosome. Microsc. Microanal. 25, 1052–1060. https://doi.org/10.1017/S1431927619014557.

Aich, A., Afrin, L.B., Gupta, K., 2015. Mast cell-mediated mechanisms of nociception. Int. J. Mol. Sci. 16 (12), 29069–29092. https://doi.org/10.3390/ijms161226151.

Alberts, B., Johnson, A., Lewis, J., Raff, M., Roberts, K., Walter, P., 2002. Molecular Biology of the Cell. Garland Science Sensory Epithelia, New York.

Albrecht, J., Kopietz, R., Frasnelli, J., Wiesmann, M., Hummel, T., Lundstrom, J.N., 2010. The neuronal correlates of intranasal trigeminal function-an ALE meta-analysis of human functional brain imaging data. Brain Res. Rev. 62, 183–196. https://doi.org/10.1016/j.brainres rev.2009.11.001.

Bancroft, J.D., Stevens, A.A., 1997. Theories and practice of histological technique. Churchill Living Stone, Livingstone Edinburgh, London, New York, pp. 109–145.

Banks, W.J., 1993. Applied Veterinary Histology. Mosby-Year Book, St. Louis.

Boyle, J.A., Heinke, M., Gerber, J., Frasnelli, J., Hummel, T., 2007. Cerebral activation to intranasal chemosensory trigeminal stimulation. Chem. Senses 32, 343–353. https://doi.org/10.1093/chemse/bjm004.

Brechbuhl, J., Klaey, M., Broillet, M.C., 2008. Grueneberg ganglion cells mediate alarm pheromone detection in mice. Science 32, 1092–1095. https://doi.org/10.1126/science.1160770.

Chatterjea, D., Martinov, T., 2015. Mast cells: versatile gatekeepers of pain. Mol. Immunol. 63 (1), 38–44. https://doi.org/10.1016/j.molimm.2014.03.001.

Chen, C.R., Kachramanoglou, C., Li, D., Andrews, P., Choi, D., 2014. Anatomy and Cellular Constituents of the Human Olfactory Mucosa: A Review Journal of Neurological Surgery-Part B 75, 293–300. https://doi.org/10.1055/s-0033-1361837.

Dustin, M.L., Colman, D.R., 2002. Neural and immunological synaptic relations. Science 298, 785–789. https://doi.org/10.1126/science.1076386.

Eshrah, A.E., 2017. The Camel Rhinarium: A study revealing the presence of the nasal plane in dromedary camel (Camelus dromedarius), with special reference to its epidermal structure. Anat. Histol. Embryol. 46, 65–72. https://doi.org/10.1111/ahe.12238.

Eshrah, E.A., Kassab, A.A., 2019. Scanning electron microscopy and histomorphology of the epiglottis in dromedaries: A study revealing unusual structure with the probable functional role. Microsc. Res. Tech. 82, 1353–1358. https://doi.org/10.1002/jemt.23287.

Farbman, A.I., 1992. Cell Biology of Olfaction Cambridge University Press.

Fawcett, D. W., Jensh, R. P., 1997. Bloom and Fawcett, concise histology. 2nd Ed Champman and Hall USA. DOI: 10.1046/j.1365-2303.1998.0097e.x

Fischer, A.H., Jacobson, K.A., Rose, J., Zeller, R., 2008. Hematoxylin and eosin staining of tissue and cell sections. CSH Protocols. https://doi.org/10.1101/pdb.prot4986.

Fleischer, J., Schwarzenbacher, K., Besser, S., et al., 2006. Olfactory receptors and signalling elements in the Grueneberg ganglion. J. Neurochem. https://doi.org/10.1111/j.1471-4159.2006.03894.x.

Fuss, S.H., Omura, M., Mombaerts, P., 2005. The Grueneberg ganglion of the mouse projects axons to glomeruli in the olfactory bulb. Eur. J. Neurosci. 22, 2649–2654. https://doi.org /10.1111 /j.1460-9568.2005.04468.x

Giannetti, N., Saucier, D., Astic, L., 1992. Organization of the septal organ projection to the main olfactory bulb in adult and newborn rats. J. Comp. Neurol. 323, 288–298. https://doi.org/10.1002/cne.903230211.

Grosmaitre, X., Fuss, S.H., Lee, A.C., et al., 2009. SR1, a mouse odorant receptor with an unusually broad response profle. J. Neurosci. 29, 14545–14552. DOI: 10.1523/jneurosci.2752-09.2009

Grosmaitre, X., Santarelli, L.C., Tan, J., et al., 2007. Dual functions of mammalian olfactory sensory neurons as odor detectors and mechanical sensors. Nat. Neurosci. 10, 348–354. DOI: 10.1038/nn1856

Hansen, A., 2007. Olfactory and solitary chemosensory cells: two different chemosensory systems in the nasal cavity of the American alligator, Alligator mississippiensis. B.M.C. Neurosci. 8, 64. https://doi.org/10.1186/1471-2202-8-64.

Hansen, A., Zeiske, E., 1998. The peripheral olfactory organ of the zebrafish, Danio rerio: An ultrastructural study. Chem. Senses 23(1), 39- 48. DOI: 10.1093/chemse/23.1.39

Iannilli, E., Del Gratta, C., Gerber, J.C., Romani, G.L., Hummel, T., 2008. Trigeminal activation using chemical, electrical, mechanical stimuli. Pain 139, 376–388. https://doi.org/10.1016/j.pain.2008.05.007.

Kociánová, A., Gorošová, Tichý, F., Čížek, P., Machálka, M., 2006. Structure of Masera's Septal Olfactory Organ in Cat (Felis silvestris f. catus) - Light

Microscopy in Selected Stages of Ontogeny. Acta. Vet. Brno. 75, 471–475. DOI: 10.2754/avb200675040471

Krasteva, G., Kummer, W., 2012. "Tasting" the airway lining fluid. Histochem. Cell. Biol. 138, 365–383. https://doi.org/10.1007/s00418-012-0993-5.

Kratzing, J.E., 1984. The structure and distribution of nasal glands in four marsupial species. J. Anat. 139, 553–564. PMCID: PMC1165068

Kubota, Y., Karube, F., Nomura, M., Kawaguchi, Y., 2016. The diversity of cortical inhibitory synapses. Front. Neural. Circuits. 10, 27. https://doi.org/10.3389/fncir.2016.00027.

Llewellyn McKone, W., 1997. Osteopathic Athletic Health Care: Principles and practice, springer, 1st Ed, pp. 147

Lötsch, J., Oertel, B.G., Felden, L., Nöth, U., Deichmann, R., Hummel, T., Walter, C., 2020. Central encoding of the strength of intranasal chemosensory trigeminal stimuli in a human experimental pain setting. Hum. Brain Mapp. 41, 5240–5254. https://doi.org/10.1002/hbm.25190.

Lundström, J.N., Boesveldt, S., Albrecht, J., 2011. Central processing of the chemical senses: an overview. ACS Chem. Neurosci. 2, 5–16. https://doi.org/10.1021/cn1000843.

Ma, M., Grosmaitre, X., Iwema, C.L., Baker, H., Greer, C.A., Shepherd, G.M., 2003. Olfactory signal transduction in the mouse septal organ. J. Neurosci. 23, 317–324. https://doi.org/10.1523/jneurosci.23-01-00317.2003.

Mamasuew, K., Breer, H., Fleischer, J., 2008. Grueneberg ganglion neurons respond to cool ambient temperatures. Eur. J. Neurosci. 28, 1775–1785. https://doi.org/10.1111/j.1460-9568.2008.06465.x.

Mamasuew, K., Michalakis, S., Breer, H., et al., 2010. The cyclic nucleotide-gated ion channel CNGA3 contributes to coolness-induced responses of Grueneberg ganglion neurons. Cell. Mol. Life Sci. 67, 1859–1869. https://doi.org/10.1007/s00018-010-0296-8.

Marshall, D.A., Maruniak, J.A., 1986. Masera's organ responds to odorants. Brain Res. 366, 329–332. https://doi.org/10.1016/0006-8993(86)91312-0.

Nomura, T., Takahashi, S., Ushiki, T., 2004. Cytoarchitecture of the normal rat olfactory epithelium: Light and scanning electron microscopic studies. Arch. Histol. Cytol. 67, 159–170. https://doi.org/10.1679/aohc.67.159.

Pinho-Ribeiro, F.A., Verri Jr, W.A., Chiu, I.M., 2017. Nociceptor Sensory Neuron-Immune Interactions in Pain and Inflammation. Trends Immunol. 38, 5–19. https://doi.org/10.1016/j.it.2016.10.001.

Seifert, F., Maihofner, C., 2009. Central mechanisms of experimental and chronic neuropathic pain: findings from functional imaging studies. Cell Mol. Life Sci. 66, 375–390. https://doi.org/10.1007/s00018-008-8428-0.

Sekizawa, S.I., Tsubone, H., 1994. Nasal receptors responding to noxious chemical irritants. Resp. Physiol. 96, 37–48. https://doi.org/10.1016/0034-5687(94)90104-x.

Siegrist, G., Dolivo, M., Dunant, Y., Foroglou-Kerameus, C., De Ribaupierre, F.R., Rouiller, C.H., 1968. Ultrastructure and function of the chromaffin cells in the superior cervical ganglion of the rat. J. Ultrastructure Res. 25, 381–407. https://doi.org/10.1016/S0022-5320(68)80093-0.

Smith, T.D., Bhatnagar, K.P., Shimp, K.L., Kinzinger, J.H., Bonar, C.J., Burrows, A.M., Mooney, M.P., Siegel, M.I., 2002. Histological definition of the vomeronasal organ in humans and chimpanzees, with a comparison to other primates. Anat. Rec. 267, 166–176. https://doi.org/10.1002/ar.10095.

Storan, M.J., Key, B., 2006. Septal organ of Gruneberg is part of the olfactory system. J. Comp. Neurol. 494, 834–844. https://doi.org/10.1002/cne.20858.

Taniguchi, K., Tohru, A.R., Kazushige, O., 1993. Fine structure of the septal olfactory organ of masera and its associated gland in the golden hamster. J. Vet. Med. Sci. 55, 107–116. https://doi.org/10.1292/jvms.55.107.

Tomiyasu, J., Kondoh, D., Sakamoto, H., Matsumoto, N., Haneda, S., Matsui, M., 2018. Lectin histochemical studies on the olfactory gland and two types of glands in vomeronasal organ of the brown bear. Acta Histochem. 120, 566–571. https://doi.org/10.1016/j.acthis.2018.07.003.

Tomiyasu, J., Kondoh, D., Sakamoto, H., Matsumoto, N., Sasaki, M., Kitamura, N., Haneda, S., Matsui, M., 2017. Morphological and histological features of the vomeronasal organ in the brown bear. J. Anat. 231, 749–757. https://doi.org/10.1111/joa.12673.

Weiler, E., Farbman, A.I., 2003. The septal organ of the rat during postnatal development. Chem. Senses 28, 581–593. https://doi.org/10.1093/chemse/bjg047.

Widdicombe, J.H., Wine, J.J., 2015. Airway gland structure and function. Physiol. Rev. 95, 1241–1319. https://doi.org/10.1152/physrev.00039.2014.

Wu, S.M., 2010. Synaptic organization of the vertebrate retina: general principles and species-specific variations: the Friedenwald lecture. Invest. Ophthalmol. Vis. Sci. 51, 1263–1274. https://doi.org/10.1167/iovs.09-4396.